SEARCHING FOR DARK MATTER IN PARTICLE PHYSICS EXPERIMENTS

A Senior Honors Thesis

by

PAUL BRIAN GEFFERT

Submitted to the Office of Honors Programs
Texas A&M University
in partial fulfillment of the requirements of the

UNIVERSITY UNDERGRADUATE
RESEARCH FELLOWS

April 2008

Double Degree: Physics and Mathematics

ABSTRACT

Searching for Dark Matter in Particle

Physics Experiments (April 2008)

Paul B. Geffert
Department of Physics
Texas A&M University

Fellows Advisor: Dr. David Toback
Department of Physics

Astronomical observations have shown that the amount of visible matter in the universe comprises only a fraction of the total mass of the universe. This extra mass is described as "dark matter". In this thesis we search for evidence of a new type of particle that would be the dark matter in the universe and decay from heavy, long-lived supersymmetric particles produced in high energy $p\overline{p}$ collisions. Since our particles have a long lifetime and decay into a photon and a $\widetilde{G}$, our dark matter candidate and the supersymmetric partner of the graviton, we search for evidence of photons that arrive delayed in time. This thesis explores a new search technique and uses data from run II of the Fermilab Tevatron. We observe 24 events which is roughly consistent with our background expectation of 18.1 ± 4.2 events.

ACKNOWLEDGMENTS

This work was supported, in part, by funds from the Office of Honors Programs. Many thanks to Peter Wagner, Max Goncharov, Eunsin Lee, and my advisor Dr. David Toback, without whom my thesis would not have been possible. Finally, thank you to both of my parents for being constant sources of advice and encouragement.

TABLE OF CONTENTS

CHAPTER Page

LIST OF FIGURES

FIGURE Page

LIST OF TABLES

CHAPTER I

INTRODUCTION*

Recent astronomical observations from experiments such as the Wilkinson Microwave Anisotropy Probe (WMAP) [1] have indicated that the visible matter in the universe comprises only a fraction of the universe's total energy. From these observations we also know there there must exist additional unseen matter, called dark matter, that accounts for about 23% of the energy of the universe. Predating WMAP, the first astronomical indications of the presence of undetected matter in the universe were the highly anomalous orbital velocities of stars about the centers of galaxies [2]. Dark matter is so named because it does not interact electromagnetically, i.e. does not interact with the light we see, and has yet to be directly detected. The known particles of the standard model (SM) [3] of particle physics only account for 4% of the total energy of the universe and therefore are not the dark matter [1].

While there are multiple physical theories that could account for this dark matter, the leading such theory is Supersymmetry (SUSY) [4], an extension to the accepted standard model of particle physics [3]. Supersymmetry was originally created in response to the problems that exist with the theoretical underpinnings of the standard model. SUSY postulates that each SM particle has a corresponding supersymmetric partner. If SUSY is correct, one of the particles predicted in the model could be the dark matter.

In this thesis we assume a model of a gauge mediated supersymmetry breaking (GMSB) [5]. These models are experimentally motivated because they explain the observation of an anomalous $ee\gamma\gamma\not{E}_T$ [6, 7] candidate event in the Collider Detector

*This thesis follows the style of *Physical Review D.*

at Fermilab (CDF) during Run I of the Fermilab Tevatron. From a theoretical perspective, we use GMSB because it provides a good warm dark matter candidate [8]. Warm dark matter is so named because it is much lighter and hence faster moving than other theorized of dark matter particles. Warm dark matter has the ability to much better account for the small scale structure of galaxies than other heavier dark matter candidates. In our GMSB model, the gravitino ($\widetilde{G}$), the supersymmetric partner of the yet undiscovered graviton, is the lightest supersymmetric particle (LSP). We assume R-parity, a quantum mechanical number that describes supersymmetric particles, to be conserved in this analysis, in which case gravitinos will not decay and will be stable forever.

In this thesis, we attempt to discover evidence for GMSB SUSY in high energy $p\bar{p}$ collisions at the Fermilab Tevatron, from pair production of SUSY particles that promptly decay into a pair of neutralinos $\widetilde{\chi}_1^0$, the next-to-lightest supersymmetric particle (NLSP). In our model these NLSPs can have a nanosecond lifetime and then decay into a photon (γ) and a $\widetilde{G}$. We search for evidence of photons from heavy long-lived neutralinos in the Collider Detector at Fermilab (CDF) using photon timing to find delayed photons. We attempt to improve upon a previous search [9], from which many of the details of the analysis presented here are modeled.

Our photon time variable is

$$t_{\rm corr} \equiv (t_f - t_i) - \frac{|\vec{x}_f - \vec{x}_i|}{c}, \tag{1.1}$$

where $t_f - t_i$ is the time between the collision t_i and the arrival time t_f of the photon at the calorimeter, and $|\vec{x}_f - \vec{x}_i|$ is the distance between the position where the photon hits the detector and the collision point. As $t_{\rm corr}$ is corrected for the collision time and the time-of-flight, we expect promptly produced photons to have an average $t_{\rm corr}$ of 0 and photons from long-lived particles to have $t_{\rm corr} > 0$, on average.

Figure 1 illustrates the decay of a $\widetilde{\chi}_1^0$ into a photon and a $\widetilde{G}$. The $\widetilde{\chi}_1^0$ emanates a gravitationally interacting $\widetilde{G}$, which therefore leaves undetected, and a photon after traveling a macroscopic distance inside the detector. The photon's arrival time at the calorimeter is "delayed" compared to a prompt photon that would propagate directly from the collision to the same position at the calorimeter.

Along with a delayed photon, Ref. [9] searched for missing transverse energy ($\not\!\!E_T$) in the final state, the majority of which arises from weakly interacting $\widetilde{\chi}_1^0$'s and/or gravitationally interacting $\widetilde{G}$'s which therefore leave the detector. It also searched for a jet, which is a grouping of energy in the calorimeter, and a reconstructed vertex, which comes from matching multiple tracks together in both position and time. (We shall refer to this analysis as the $\gamma + \not\!\!E_T$ + jet analysis from here forward.) We simplify these final state requirements and search for events with at least one delayed photon, $\not\!\!E_T$, and at least one isolated track, where we define the isolation of a track as the Σp_{T} of all tracks that are "close" in both time and position. We use the t_0 and z_0, the initial time and position respectively, of the highest p_T isolated track to determine the collision time and position and therefore the fully corrected photon time, t_{corr}. Other searches for heavy, long-lived neutralinos have been performed at LEP [10]. This analysis follows the prescription in Ref. [11] for neutralinos with long lifetimes.

This search is performed at the Collider Detector at Fermilab, a general purpose particle detector at the Fermilab Tevatron. A description of this detector can be found in [12]. One key aspect of CDF that makes photon timing possible is the electromagnetic (EM) calorimeter ("EMTiming") [13] system that was built in response to the $ee\gamma\gamma\not\!\!E_T$ event, in particular to verify that all the EM objects were from the primary collision. The timing information can provide evidence to distinguish between whether an event is from some non-collision background source or perhaps actually the decay product of a long-lived particle that decayed to a photon

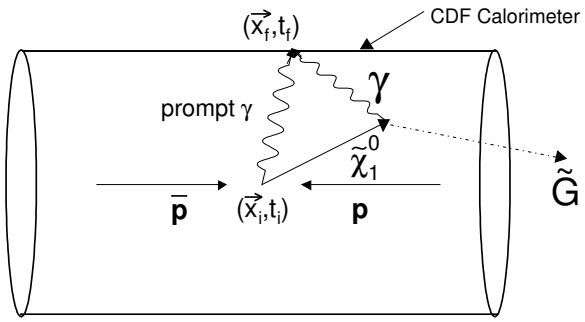

FIG. 1: The schematics of the GMSB process of a long-lived $\widetilde{\chi}_1^0$ decaying into a $\widetilde{G}$ and a photon inside the CDF detector. While the $\widetilde{G}$ leaves the detector the photon travels to the detector wall and deposits energy in the EM calorimeter. A prompt photon would travel directly to the detector walls. Relative to the collision vertex time, the photon from the $\widetilde{\chi}_1^0$ would appear "delayed" in time. Note that the lifetime of the $\widetilde{\chi}_1^0$ may be long enough for it to leave the detector, giving rise to additional $\not\!\!E_T$.

or electron.

Theoretically, mainly GMSB models predict long-lived, heavy, neutral particles in the form of $\widetilde{\chi}_1^0$'s with a mass of $\sim$100 GeV and a lifetime on the order of nanoseconds that decay to photons. At the Tevatron, gaugino pair-production dominates the sparticle production and each produces pairs of $\widetilde{\chi}_1^0$'s. Each $\widetilde{\chi}_1^0$ decays into a $\widetilde{G}$, that gives rise to $\not\!\!E_T$ if the decay occurs inside the calorimeter, and a photon. The likelihood of a $\widetilde{\chi}_1^0$ decaying inside the detector is dependent upon its lifetime. With differing lifetime, the probabilities of observing zero, one or two photons from the $\widetilde{\chi}_1^0$ decays vary.

The main difference between this analysis and [9] is that we require an isolated track while the $\gamma + \not\!\!E_T +$ jet analysis requires both a jet and a reconstructed vertex. By removing these two requirements, we eliminate the systematic uncertainties associated with reconstructing jets and collisions. To motivate our isolated track requirement, we consider the dominant production processes shown in Fig. 2. In

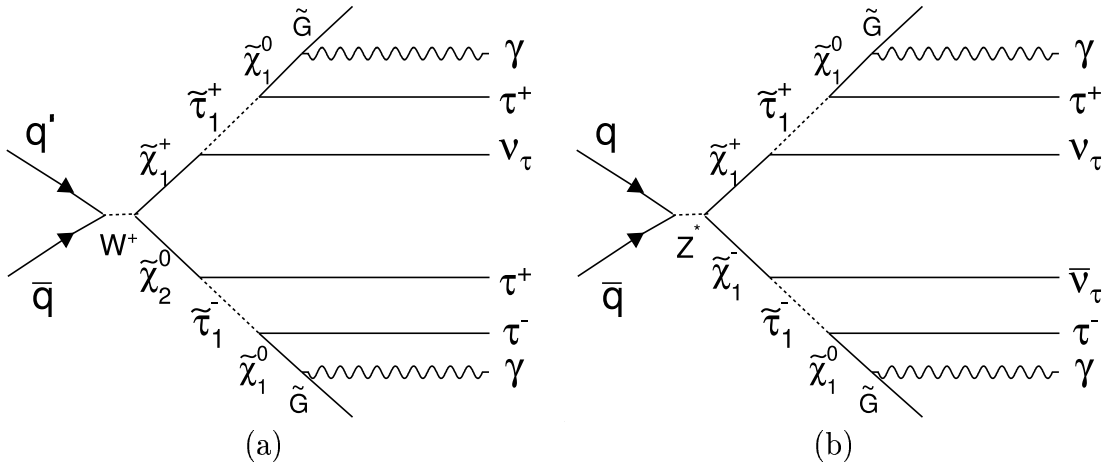

FIG. 2: Feynman diagrams of the dominant tree production processes at the Tevatron for the GMSB model line we consider: $\widetilde{\chi}_1^{\pm}$ $\widetilde{\chi}_2^0$ (45%) (a) and $\widetilde{\chi}_1^{\pm}$ pair (b) production (25%). The τ's, if available, can be identified in the calorimeter as isolated tracks. Note that we only show one choice for the charge. The remaining processes are slepton (τ_1, e_R, μ_R) pair production.

both diagrams, we see that one or more taus are produced as a result of the decay chains. Ignoring contamination from other collisions, these taus can decay via $\tau \to e\nu\nu$, $\tau \to \mu\nu\nu$, or $\tau \to \pi^{\pm}\nu$ and therefore have the signature of a single isolated track which would pass an isolation requirement. This isolated track indicates the position and time of the collision in the event and therefore effectively replaces the reconstructed vertex requirement. Additionally, we retain sensitivity to other models that produce leptons in decay chains that result in long lived $\widetilde{\chi}_1^0$s. In this manner, our search exhibits a degree of model independence and complementarity to the $\gamma + \not\!\!E_T +$ jet search.

The isolated track requirement is effective at reducing the main background in the $\gamma + \not\!\!E_T +$ jet search, which is SM collisions. Standard model collisions are much more likely to produce jets with many closely correlated tracks due to quark hadronization than lone isolated tracks. Therefore, our simple isolated track requirement will have a powerful effect in reducing SM backgrounds.

In this analysis we will focus on the $\gamma + \not\!\!E_T$ case which is more sensitive to higher lifetimes [11]. We perform a blind analysis in the sense that we blind the signal region and select the final event requirements based on the signal and background expectations alone. The backgrounds are estimated from the photon timing shape using control regions from the same γ+isolated track+$\not\!\!E_T$ dataset. We use GMSB models to estimate the signal expectations. Before unblinding the signal region we find our final event requirements by optimizing our sensitivity for the lowest expected 95% C.L. expected cross section limits in the $\widetilde{\chi}_1^0$ mass and lifetime region that we are sensitive to. We present cross section limits so that exclusion regions in the GMSB parameter space can be determined when the signal region is unblinded. The exclusion limits in the $\widetilde{\chi}_1^0$ mass-lifetime space from the $\gamma + \not\!\!E_T +$ jet analysis we are attempting to improve are shown in Fig. 3 (also shown are the LEP limits [10]).

The structure of this thesis is outlined here and follows that of Ref. [14]. We acknowledge some of the text, as well, is taken with permission from this source. We will indicate wherever we have done so. Chapter II explains the GMSB models in more detail. Chapter III describes the search strategy, the dataset and the baseline event selection. Chapter IV outlines the different backgrounds and how we estimate them for use in the optimization procedure. Chapter V describes the Monte Carlo (MC) that we use to model the signal acceptance. The optimization procedure, and its result, are shown in Ch. VI. We unblind the signal region in Ch. VII and compare our data to expectations. We conclude in Ch. VIII.

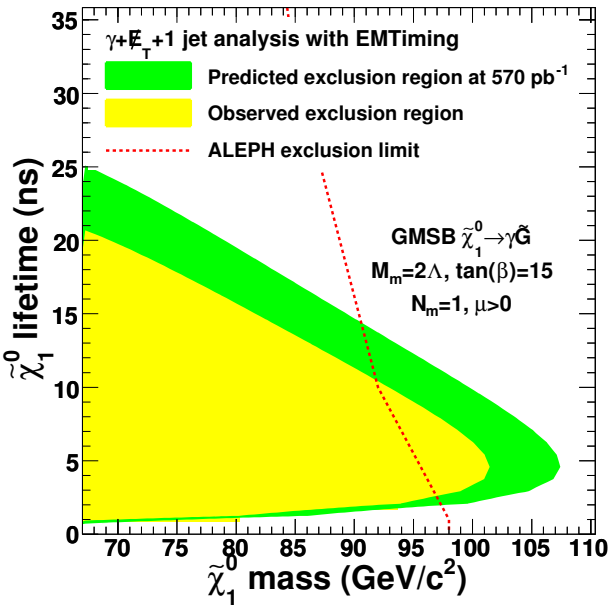

FIG. 3: The exclusion region from the $\gamma + \not\!\!E_T +$ jet delayed photons analysis as a function of $\tilde{\chi}_1^0$ mass and lifetime for the Snowmass Slope-choice of parameters [15]. Also shown are the limits from GMSB searches at ALEPH/LEP [10]. This figure is taken from Fig. 25 in Ref. [9].

CHAPTER II

THEORY

GMSB is a major theory that predicts heavy, neutral, long-lived particles that decay to photons. It has 6 free parameters that are well described in the literature [5]: the supersymmetry breaking scale, Λ, the messenger mass scale, $M_{\rm M}$, the ratio of the Higgs vacuum expectation values, $\tan(\beta)$, $\mathrm{sgn}(\mu)$, the number of messenger fields, $N_{\rm M}$, and the $\widetilde{G}$ mass factor, $c_{\rm Grav}$. In these models the NLSP is either the stau ($\widetilde{\tau}$) or the $\widetilde{\chi}_1^0$. For concreteness we use the Snowmass Slope constraint (SPS 8) [15] that is commonly used [10, 16] to reduce the number of free parameters from 6 to 2: the $\widetilde{\chi}_1^0$ mass and lifetime. We will focus on the $\widetilde{\chi}_1^0$-NLSP case here, for which the branching ratio is $\sim$100% to decay to a photon and a $\widetilde{G}$. At the Tevatron $\widetilde{\chi}_1^0$'s are mostly pair produced as end products of cascade decays from a chargino, $\widetilde{\chi}_1^\pm$, pair ($\sim$45%) or a $\widetilde{\chi}_1^\pm$ and a $\widetilde{\chi}_2^0$ ($\sim$25%) [17]. The major production channels are shown in Fig. 2. For much of the parameter space the $\widetilde{\chi}_1^0$ can be long-lived, with a decay time on the order of nanoseconds which corresponds to decay lengths of meters. The $\widetilde{\chi}_1^0$ can decay inside the detector or, in a fraction of cases, leave the detector volume before it decays.

Table 1 shows the GMSB model parameters, the resulting $\widetilde{\chi}_1^0$ mass and lifetime, and the next-to-leading-order (NLO) production cross section for example points. The production cross sections are calculated to leading-order using PYTHIA [18] with the NLO corrections using the K-factors shown in Figure 4 as a function of $\widetilde{\chi}_1^0$ masses for $\widetilde{\chi}_1^\pm$ pair and $\widetilde{\chi}_1^\pm$ $\widetilde{\chi}_2^0$ production [19]. The values range around 1.1-1.3 for the mass range considered. The production cross section is independent of the $\widetilde{\chi}_1^0$ lifetime, as this only scales with the $\widetilde{G}$ mass for a fixed $\widetilde{\chi}_1^0$ mass [5]. We use the total production cross section to estimate our sensitivity as it produces the best limits [20].

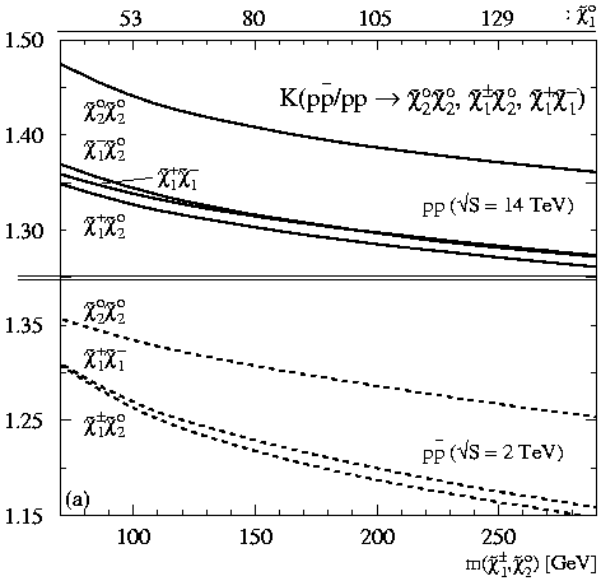

FIG. 4: The K-factors for use in modifying the LO production cross sections of $\widetilde{\chi}_1^\pm$ pair and $\widetilde{\chi}_1^\pm$ $\widetilde{\chi}_1^0$ production from PYTHIA as a function of the average mass of the $\widetilde{\chi}_1^\pm$ and $\widetilde{\chi}_2^0$ which are almost identical in the scenario chosen in Ref. [19]. The figure is taken from Fig. 3a therein. For convenience we plotted the $\widetilde{\chi}_1^0$ mass as a second x-axis, taken from Fig. 3b therein.

$m_{\widetilde{\chi}}$ (GeV/c^2)	$\tau_{\widetilde{\chi}}$ (ns)	$m_{\widetilde{G}}$ (eV/c^2)	Λ (GeV)	K-factor	NLO $\sigma_{\rm prod}$ (pb)
67	10	121	51500	1.23	1.26
80	10	199	60500	1.21	0.518
80	20	280	60500	1.21	0.518
100	5	248	74000	1.19	0.162

TABLE 1: Examples for $\widetilde{\chi}_1^0$ masses and lifetimes relevant for this analysis and their translation to the SUSY parameters in accordance with the GMSB Snowmass Slope SPS 8 [15], and the NLO production cross sections. Note the different unit for the $\widetilde{G}$ mass.

CHAPTER III

OUTLINE OF THE SEARCH AND DATA SETS

A. Overview

This analysis is begun by gathering a dataset of events with central high-E_T EM-object and $\not\!\!E_T$ as these are candidates for photons and $\not\!\!E_T$ from $\widetilde{\chi}_1^0$ decays (this is the same procedure as in Ref. [9]). This set of events is then searched for a good photon, large $\not\!\!E_T$ and at least one high-p_T track, presumably from a τ that is part of the cascade decays of $\widetilde{\chi}_1^\pm$ and/or $\widetilde{\chi}_2^0$. Then we apply a baseline set of requirements to remove the dominant background sources as described in Sec. III.C. The final signal region is defined by further kinematic requirements (cuts), described in Ch. VI, and finally a cut on the fully corrected photon arrival time. The cuts that differ between the search in Ref. [9] and this thesis are summarized in Table **??**. The number of background events inside this timing window is estimated using a fit of the known shapes of the backgrounds in control regions outside the window of the same dataset as described in Ch. IV.

In Ch. VI we optimize our predicted sensitivity using a simulation of the event distribution in the signal region from the GMSB model (see Ch. V) and calculate, for a GMSB parameter point, the lowest expected 95% C.L. cross section limit as a function of the following event variables: Photon E_T, $\not\!\!E_T$, isolated track p_T, track isolation and $t_{\rm corr}$. After the optimization we are left with an optimal set of requirements that we apply to the unblinded signal region. We next describe the dataset that is used for the baseline selection.

Cuts Only in Ref. [9]	Cuts Only in This Thesis
At least one jet	Isolated track
Reconstructed vertex	
Difference in ϕ between the $\not\!\!E_T$ and jet	

TABLE 2: A summary of the different cuts used in Ref. [9] and this thesis.

B. Initial Data Set

During data taking at CDF, events are selected in real time that have an EM-object in the central calorimeter and $\not\!\!E_T$ above a certain threshold. Only events that occur after the EMTiming system became fully functional are considered, which corresponds to a total luminosity of (570±34) pb^{-1} in this analysis.

C. Baseline Event Selection

From the initial dataset, we create a baseline sample of γ+track+$\not\!\!E_T$ events. We require one central photon with a corrected E_T>30 GeV which is where the requirements for our initial data set become fully efficient. We select the highest-E_T photon in the event using the photon cuts developed in the $\gamma + \not\!\!E_T +$ jet analysis [9]. Additionally we require a raw $\not\!\!E_T$ of $\not\!\!E_T \geq 30$ GeV, where the requirements for our initial data set are fully efficient, and at least one good track that passes the requirements in Table 3 with $p_T \geq 5$ GeV/c, $|t_0| < 5$ ns, and $|z_0| < 60$ cm. We additionally use a requirement to reject events where the photon may have come from a cosmic ray muon hitting the calorimeter. This requirement rejects events with muon chamber hits within 30° in ϕ of the photon candidate that have no corresponding tracks. The full photon, track, and global event requirements that define our baseline sample are listed in Table 4. The good track selection criteria are listed in Table 3 and are

the standard cuts on COT tracks but an additional $\frac{dE}{dx}$ cut to reject slow protons. Table 5 lists the cumulative number of events which pass each of the successive cuts to create our baseline sample.

Note that we add the additional kinematic requirement of track isolation when optimizing the final event requirements. We can see in Fig. 5(a), which shows the predicted background and signal distributions with no isolation requirement, that we need the isolation requirement to better reject SM backgrounds. While the SM backgrounds have many high p_T tracks which will pass the p_T cut, isolated high p_T tracks are much less likely to occur. As we can see in Fig. 5(b), the addition of the isolation requirement improves our standard model rejection power when combined with the track p_T cut. Also, because signal events should produce 1 or more taus, which should appear as isolated tracks, our loss of acceptance is not severe.

Because the standard CDF track isolation variable may include tracks from other collisions, we have created are own isolation variable. We define a track's isolation as the Σp_T of all other tracks within 2 ns in time, 5 cm in z, and a $\Delta R = 0.4$ cone of the track that pass the cuts in Table 3. Figure 6 shows the difference in t and z between tracks from the same event. In both subfigures, the data is distributed as two different Gaussians. In each case, the Gaussian with the smaller root mean square (RMS) corresponds to tracks that originate from the same collision while the larger RMS Gaussian comes from tracks that are from a seperate collison. As we are only concerned with including tracks from the same collision we ignore the larger RMS Gaussians when estimating our effeciencies. Therefore we can see in Fig. 6 that our requirements on the difference in t and z maintian a very high effeciency for including tracks from the same collision.

Requirement
$p_T > 0.3$ GeV/c
$p_T > 1.4$ GeV/c $\|\|$ $\frac{dE}{dx} < 20$, only if charge> 0
Err$(z_0) < 1$ cm
$\|\eta\| < 1.6$
NCotStSeg(5)$\geq$2
NCotAxSeg(5)$\geq$2
$\|t_0\| < 40$ ns
$0.05 <$ Err$(t_0) < 0.8$ ns
$\|z_0\| < 120$ cm

TABLE 3: Track requirements for tracks to be considered in the isolated track selection.

Requirement
Photon
$E_T > 30$ GeV
Fiducial: $\|X_{\rm CES}\| < 21$ cm and 9 cm $< \|Z_{\rm CES}\| < 230$ cm
$E_{\rm Had}/E_{\rm Em} < 0.125$
$E^{\rm Iso}_{\rm R=0.4} < 2.0$ GeV $+ 0.02 \cdot (E_T - 20)$
$N_{\rm trks} = 0$ or $N_{\rm trks} = 1$ and $p_T < 1.0$ GeV/c $+ 0.005 \cdot E_T$
$\Sigma p_{\rm T}$ of tracks in the $\Delta R = 0.4$ cone < 2.0 GeV/c $+ 0.005 \cdot E_T$
$E^{\rm cluster}_{\rm 2nd\ strip\ or\ wire} < 2.4$ GeV $+ 0.01 \cdot E_T$
PMT asymmetry: $\frac{\|E_{\rm PMT1} - E_{\rm PMT2}\|}{E_{\rm PMT1} + E_{\rm PMT2}} < 0.6$
Track
Passes cuts in Table 3
$p_T>5$ GeV/c
$\|z_0\| < 60$ cm
$\|t_0\| < 5$ ns
Global Event Cuts
raw $\not\!\!E_T > 30$ GeV
Passes cosmic ray rejection requirement

TABLE 4: The photon, track, and global event cuts used to select the baseline sample of γ+isolated track+$\not\!\!E_T$ events. Note that we use the photon ID requirements described in [9]. We use the track requirements shown in Table 3. The cosmic ray rejection is explained in [21]. The number of events in the data that pass each cut are shown in Table 5, the estimated signal acceptance in Table 7.

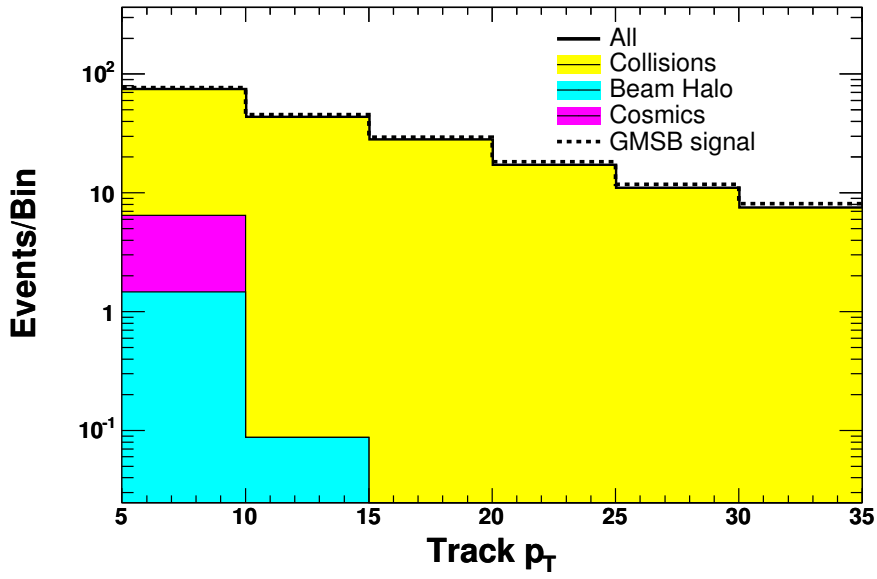

(a)

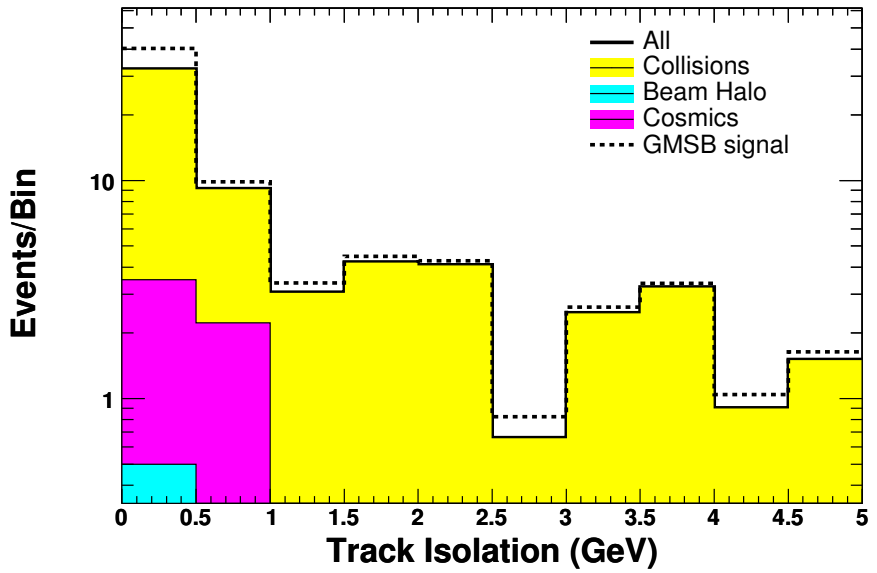

(b)

FIG. 5: The predicted shapes of the background and signal when (a) no track isolation requirement is used and (b) when a track isolation requirement is implemented. It is clear that a simple p_T cut does not effectively discriminate between the signal and background.

Selection	No. of Observed Events
$E_T > 30$ GeV, $\not\!\!E_T > 30$ GeV, photon ID cuts	120263
Good track with $p_T > 5$ GeV/c, $\|z_0\| < 60$ cm, and $\|t_0\| < 5$ ns	14204
Cosmics rejection	13877

TABLE 5: Event reduction for the baseline γ+isolated track+$\not\!\!E_T$ dataset. For the individual requirements see Table 4.

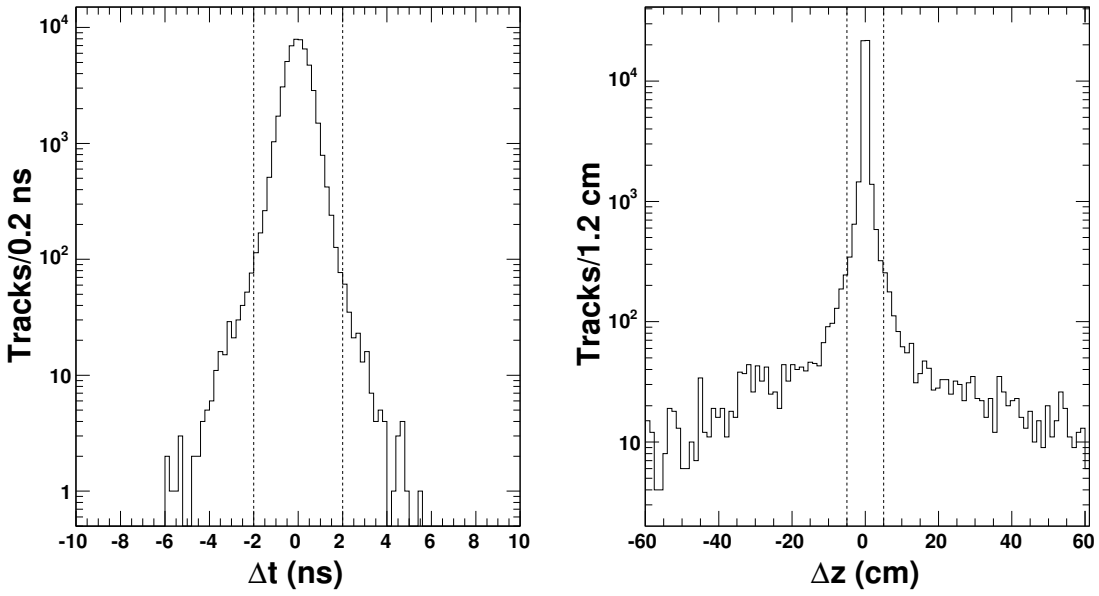

(a) (b)

FIG. 6: The difference int t (a) and z (b) between the leading track in events in our pre-selection sample and all of the other good tracks in the same event that pass the cuts in Table 3. These show our effeciency for including tracks from the same collision into the track isolation calculation. We denote with dotted lines that we take t within 2 ns and z within 5 ns in our track isolation calculations. In both subfigures, the secondary higher RMS Gaussian corresponds to tracks from a different collision.

CHAPTER IV

BACKGROUND METHODS

This section describes the various background sources and the methods used to estimate them and follows the method of Ref. [14]. This analysis has two major background sources: photon candidates produced by non-collision sources of two seperate types and photon candidates from standard model collisions. We seperate each type and create timing control templates that we utilize in the background estimation fit.

We produce backgound estimates (as well as signal acceptance estimates, see Ch. V) for a wide variety of sets of kinematic and timing requirements. These estimates are used in the optimization procedure described in Ch. VI. The final kinematic requirements found by this optimization are also described in Ch. VI.

A. Non-Collision Backgrounds

There are two types of non-collision backgrounds for our analysis. They are arise from (1) cosmic ray muons producing a photon candidate in the calorimeter (cosmics) and (2) beam related issues that create muons that travel parallel to the beam, producing a photon candidate in the EM calorimeter (beam halo).

To estimate the background contribution of each non-collision type, we seperate the two in exactly the same manner as in Ref. [14] to create their time shape templates shown in Fig. 7(b) and (c). As explained in [9], [-20,-6] ns is dominated by beam halo while [25,90] ns is dominated by cosmics. We therefore use these two regions for our beam halo and cosmics time controll regions, respectively, in our background estimation.

Electron Requirements
$E_T > 30$ GeV and $\|\eta\| \leq 1.0$
Fiducial: $\|X_{\rm CES}\| < 21$ cm and 9 cm $< \|Z_{\rm CES}\| < 230$ cm
$0.9 < E/p < 1.1$ or $p_T > 50$ GeV/c
Track traverses $\geq$3 stereo and $\geq$3 axial COT superlayers with 5 hits each
Additional requirements to reject electrons from $\gamma \rightarrow ee$
Global Event Requirements
$\not\!\!E_T$ >30 GeV
At least one good isolated track with $p_T > 5$ GeV/c, $\|t_0\| < 5$ ns ,and $\|z_0\| < 60$ cm
Transverse mass of the electron and $\not\!\!E_T$: $50 < m_T < 120$ GeV

TABLE 6: The requirements used to select electrons from $W \rightarrow e\nu$ events to determine the right and wrong vertex $t_{\rm corr}$ background distributions. The isolated track must pass the requirements listed in Table 3. These variables are described in more detail in [12].

B. Collision Backgrounds

Collision background events can be thought of as two seperate types. The first type occurs when the photon is matched to the correct collision that produced it (right vertex). The second type arises when the photon is matched to a different collision than the one that produced it (wrong vertex).

The shape of the collision background for right and wrong vertices is estimated from $W \rightarrow e\nu$ data in order to closely mimic events with photons. The events are selected that pass the requirements summarized in Table 6. To avoid bias, the electron track is not allowed to be the leading isolated track. The resulting shapes are shown in Fig. 7(a). The distribution is fit to a double Gaussian where the smaller RMS Gaussian corresponds to a right-vertex selection and the larger RMS Gaussian corresponds to a wrong-vertex selection.

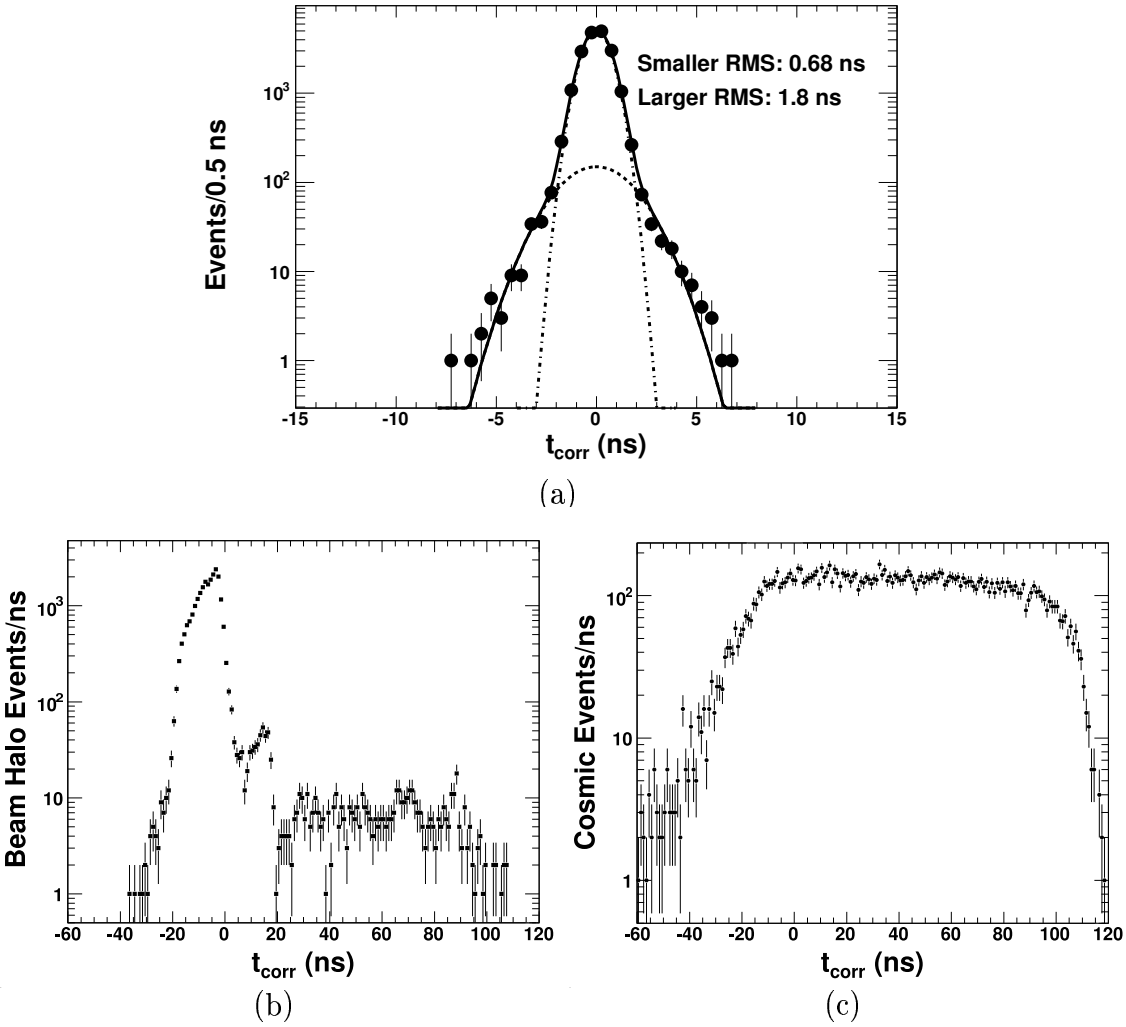

FIG. 7: The background shapes as a function of time, separated into collision (a) and non-collision (b) and(c) backgrounds. Figure (a) shows the $t_{\rm corr}$ distribution of collision data right and wrong vertex selections, as estimated using a sample of electrons from $W \to e\nu$ events passing the requirements listed in Table 6. To avoid bias, the electron track is not allowed to be the leading isolated track used to indicate the collision time and position. Figures (b) and (c) show the beam halo and cosmics background shapes, respectively.

CHAPTER V

ACCEPTANCE AND EFFICIENCIES FOR GMSB MODELS

This section describes how we estimate our signal acceptance and follows closely from [14], where a description of the MC simulation of the GMSB model can also be found. For this thesis we calculate our acceptance for a GMSB model point at $m_{\tilde{\chi}} = 100$ GeV/c^2 and $\tau_{\tilde{\chi}} = 5$ ns. We choose this point because it is near the sensitivity limit shown in Fig. 3.

The total event efficiency is used when calculating the cross section limits, and is given by:

$$A \cdot \epsilon = (A \cdot \epsilon)_{\text{Signal MC}} \times C_{\text{MC}} \tag{5.1}$$

where A is the acceptance, ϵ the efficiency and C_{MC} a correction factor to the MC simulation for small effects that are not simulated in the MC. The major effects that the MC does not simulate are (1) multiple collision effects and (2) cosmic ray backgrounds.

The leading isolated track may be associated to a collision other than the one that actually produced the photon if multiple collisions occur. This would indicate incorrectly that the extra collision is the event's main collision. To take this effect into account we simulate a fraction of the events as having fake collisions by the method in Ref. [9].

The fraction of GMSB events lost due to a cosmic ray overlapping our event and not being rejected by our cosmics rejection requirement is not simulated in the MC. This is estimated by multiplying $A \cdot \epsilon$ with the efficiency of the cosmics rejection requirement that we measure directly from our data sample. We estimate this by applying the baseline requirements on our data sample and require the photons to be within $|t_{\text{corr}}| < 10$ ns to select collision events with high purity. There are

Requirement	Events passed	$(A \cdot \epsilon)_{\text{Signal MC}}$ (%) ($m_{\tilde{\chi}} = 100$ GeV and $\tau_{\tilde{\chi}} = 5$ ns)
Sample events	120000	100.00
Central photon with $E_T > 30$, $\not\!\!E_T > 30$	68732	57.3
Photon fiducial and ID cuts	43430	36.2
Good track with $p_T > 5$ GeV/c, $\lvert z_0 \rvert < 60$ cm, and $\lvert t_0 \rvert < 5$ ns	36217	30.2
Cosmic ray rejection	N/A	29.5

TABLE 7: Summary of the event reduction for a GMSB example point in the γ+isolated track+$\not\!\!E_T$ final state as we place the baseline cuts of Table 4. Note that the cosmic ray rejection requirement is implemented as an MC correction factor, C_{MC}.

14061 events in this sample. We find that 13786 events remain after the cosmics rejection cut, giving an efficiency of $C_{\text{MC}} = 13786/14061 = (98 \pm 1)\%$, with the error conservatively overestimated.

The breakdown of events after passing each of the event and object baseline selection requirements in Table 4 for our example GMSB point at $m_{\tilde{\chi}} = 100$ GeV and $\tau_{\tilde{\chi}} = 5$ ns is shown in Table 7.

In order to estimate the sensitivity of the search we calculate the expected 95% C.L. cross section limits, which involves the uncertainties in the luminosity, background, acceptance and GMSB production cross section. For simplicity we take our systematic uncertainties to be equal to those found in Ref. [9]. To summarize, for the optimization we use a combined uncertainty of 10% on the acceptance and production cross section [22].

CHAPTER VI

OPTIMIZATION AND EXPECTED LIMITS

Using the background estimate and the signal acceptance for a given set of cuts, along with their uncertainties, the optimization procedure from Ref. [9] can be readily employed to find the optimal cuts before unblinding the signal region. We optimize for the following cuts: photon E_T, $\not\!\!E_T$, isolated track p_T, track isolation, and the lower limit on $t_{\rm corr}$, while fixing the upper limit at 10 ns. We optimize for all requirements simultaneously at our particular GMSB parameter point, $m_{\tilde{\chi}} = 100$ GeV/c^2 and $\tau_{\tilde{\chi}} = 5$ ns. We choose this parameter point as we expect our highest mass exclusion limit to be close to 100 GeV/c^2.

We optimize the cross section upper limit, $\sigma_{95}^{\rm exp}$, using the standard cross section limit calculator [22]. We take into account the predicted number of background events, the acceptance, the luminosity and their systematic uncertainties. We take

$$\sigma_{95}^{\rm exp}({\rm cuts}) = \sum_{N_{\rm obs}=0}^{\infty} \sigma_{95}^{\rm obs}({\rm cuts})\ \mathcal{P}(\mathcal{N}_{\rm obs}, \mathcal{N}_{\rm back}({\rm cuts})) \tag{6.1}$$

$${\rm RMS}^2({\rm cuts}) = \sum_{N_{\rm obs}=0}^{\infty} (\sigma_{95}^{\rm obs}({\rm cuts}) - \sigma_{95}^{\rm exp}({\rm cuts}))^2\ \mathcal{P}(\mathcal{N}_{\rm obs}, \mathcal{N}_{\rm back}({\rm cuts})). \tag{6.2}$$

Here $N_{\rm obs}$ is the number of observed events in the pseudoexperiment assuming no GMSB signal exists and $\sigma_{95}^{\rm obs}({\rm cuts})$ denotes the cross section limit if $N_{\rm obs}$ were observed. Also, $N_{\rm back}({\rm cuts})$ is the number of expected background events for a set of cuts and $\mathcal{P}(\mathcal{N}_{\rm obs}, \mathcal{N}_{\rm back}({\rm cuts}))$ is the Poisson distribution of N_{obs} with mean $N_{\rm back}({\rm cuts})$.

The expected cross section limit is then a function of the cuts that we choose to optimize for (photon E_T, $\not\!\!E_T$, isolated track p_T, track isolation, and $t_{\rm corr}$), and has at our GMSB point a minimum for the set of optimal cuts. Figure 8 shows the expected cross section limit as a function of each of the timing and kinematic requirements

	GMSB model $m_{\tilde{\chi}}$,$\tau_{\tilde{\chi}}$ (GeV/c^2, ns) 100,5
Photon E_T	30 GeV
$\not\!\!E_T$	60 GeV
Track p_T	5 GeV/c
Track Isolation	1.5 GeV/c
Lower limit on $t_{\rm corr}$	1.25 ns
Acceptance (%)	7.1±0.7
Backgrounds:	
Prompt SM	16.0±4.1
Cosmics	1.57±0.56
Beam Halo	0.50±0.18
$\sigma_{95}^{\rm exp}$ (pb)	0.324
NLO $\sigma_{\rm Signal\ MC}$ (pb)	0.162

TABLE 8: The optimized cut values for our GMSB parameter point used in the optimization.

while keeping all others fixed at their already optimized values. Note that, in reality, we optimize for all cuts simultaneously. Table 8 lists our optimization results. Our optimized cut values are: Photon E_T>30 GeV, isolated track p_T>5 GeV/c, track isolation <1.5 GeV/c, $\not\!\!E_T$>60 GeV and $t_{\rm corr}$>1.25 ns. We predict 18.1±4.1 background events with 16.02±4.10 from SM, 0.50±0.18 from beam halo and 1.57±0.56 from cosmics. For our example GMSB point at $m_{\tilde{\chi}} = 100$ GeV and $\tau_{\tilde{\chi}} = 5$ ns, we expect 6.6±0.8 signal events.

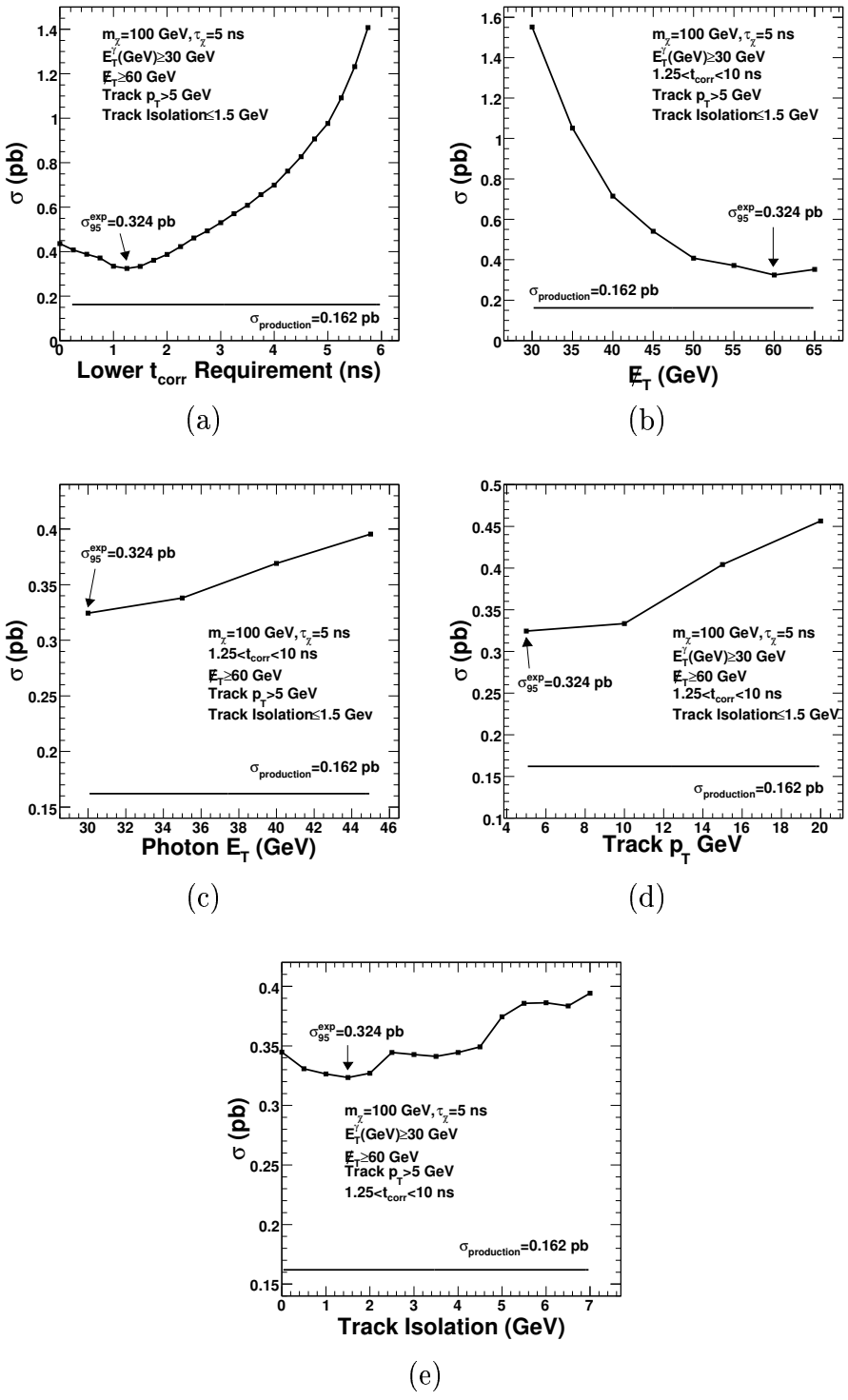

FIG. 8: The expected 95% C.L. cross section limit as a function of the $t_{\rm corr}$, the $\not\!\!E_T$, the photon E_T, track p_T, and track isolation requirements for our GMSB example point, $m_{\widetilde{\chi}} = 100$ GeV and $\tau_{\widetilde{\chi}} = 5$ ns. The arrows show the choices of the final cuts, and the expected cross section limit values.

CHAPTER VII

DATA, CROSS SECTION LIMITS, RESULTS AND CHECKS

In this section we unblind the signal region and compare our result to predictions. We observe 24 events in the final signal region, defined by the optimized cuts found in Ch. VI, and predict 18.1±4.1 background events and 6.6±0.8 signal events. As our observation is just above the error on background prediction, we do not have evidence for new physics.

Figure 9 shows the time distribution of the observed events, background prediction, and signal for our final kinematic cuts. Sub-figure (a) shows a view of the entire timing region including the background control regions and sub-figure (b) is an enlarged view of the timing signal region. Figure 10 shows the various kinematic distributions of the observed events, background prediction, and signal while holding all of the other cuts at their optimized values. In both of these figures, there is no observed event excess that points to new physics.

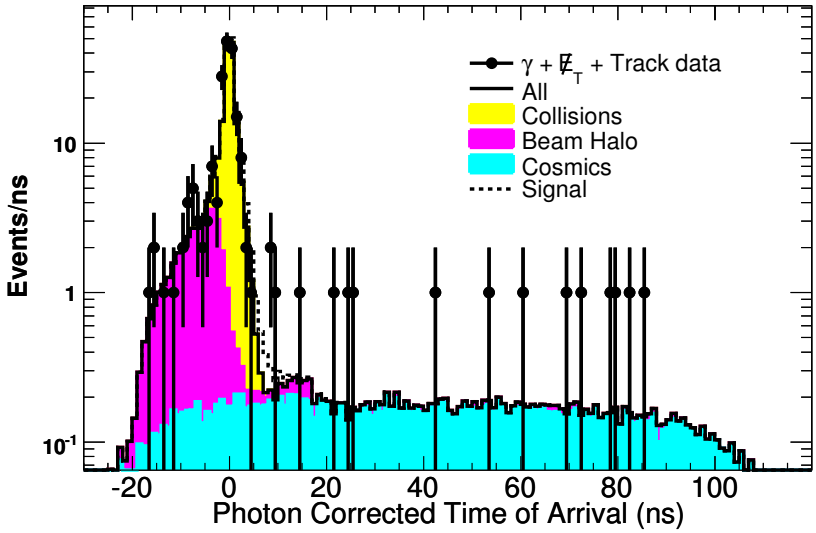

(a)

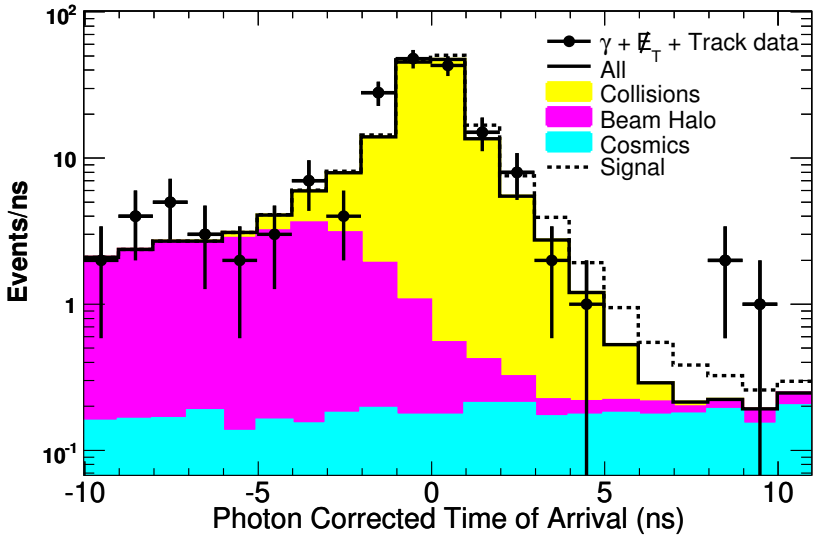

(b)

FIG. 9: The observed data and the predicted time distribution in the full time window and around the signal region, after passing the baseline and optimized kinematic cuts. We compare the observed data to the background prediction for the signal region and the GMSB signal, for an example point at $m_{\tilde{\chi}} = 100$ GeV and $\tau_{\tilde{\chi}} = 5$ ns. We predict 18.1±4.1 background events after all cuts in the signal region 1.25ns $\leq t_{\rm corr} \leq$ 10 ns. The MC is normalized to the number of expected signal events, 6.6±0.6. We observe 24 events in the signal region and therefore find to evidence of new physics.

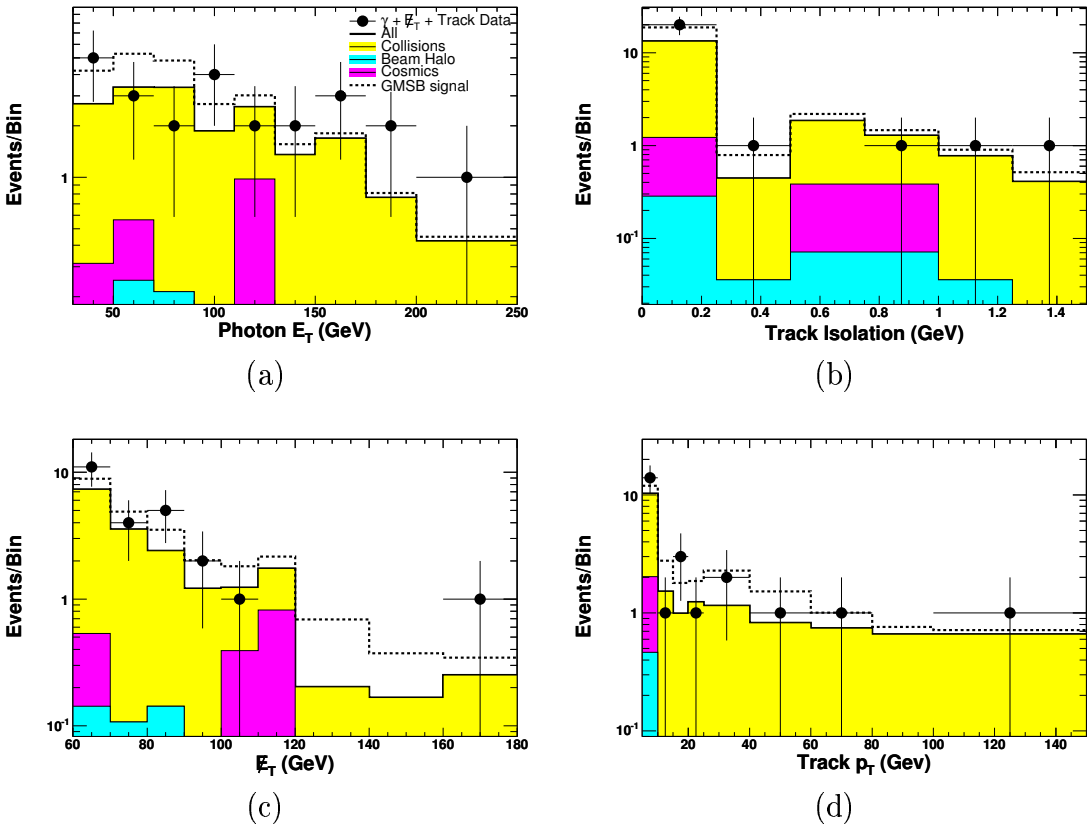

FIG. 10: The observed data and predicted kinematic distributions in the signal region after the baseline and optimized requirements. We compare the observed data to the background prediction for the signal region and the GMSB signal for our GMSB example point at $m_{\tilde{\chi}} = 100$ GeV and $\tau_{\tilde{\chi}} = 5$ ns. We predict 18.1±4.1 background events after all cuts. The MC is normalized to the number of expected signal events, 6.6±0.8. There is no evidence of new physics.

CHAPTER VIII

CONCLUSION

We have presented a search for heavy, long-lived neutralinos that decay to a photon and gravitino, a dark matter candidate, in a sample of γ+isolated track+$\not\!\!E_T$ events. To find a fully robust set of selection criteria, one would need to optimize the final event requirements for a variety of model points to study the variation in the final set of cuts.

To improve this analysis we will attempt to eliminate more SM events, by far our dominant background, and then re-optimize. To do this we will add an additional kinematic variable that represents the difference in ϕ between the $\not\!\!E_T$ and some other event object such as a jet or the highest p_T isolated track. Placing a requirement on the difference in ϕ between a jet and the $\not\!\!E_T$ will help to reject events where the $\not\!\!E_T$ arises due to a bad measurement of the jet energy in a standard model event. Another way to improve this search will be to use a larger dataset. Currently CDF has taken, but we have yet to utilize, over 2 pb^{-1} of data, which is nearly four times the data in this analysis. Hopefully, with these additions, we can set limits on the $\widetilde{\chi}_1^0$ mass and lifetime.

REFERENCES

[1] J. Dunkley *et al.*, "Five-Year Wilkinson Microwave Anisotropy Probe (WMAP) Observations: Likelihoods and Parameters from the WMAP data," *arXiv*, astro-ph/0803.0586v1, 57 pages, Mar. 2008.

[2] V. Rubin, N. Thonnard, W. K. Ford, Jr, "Rotational Properties of 21 Sc Galaxies with a Large Range of Luminosities and Radii from NGC 4605 (R=4kpc) to UGC 2885 (R=122kpc)," *Astrophysical Journal*, vol. 238, pp. 471-487, June 1980.

[3] Particle Data Group, S. Eidelman *et al.*, "Review of Particle Physics," *Phys. Lett. B*, vol. 592, pp. 1-5, July 2004.

[4] S. Martin, "A Supersymmetry Primer," *arXiv*, hep-ph/9709356, 126 pages, June 2006.

[5] M. Dine, and A. Nelson, "Dynamical supersymmetry breaking at low energies," *Phys. Rev. D*, vol. 48, pp. 1277-1287, Aug. 1993. S. Ambrosanio *et al.*, "Search for supersymmetry with a light gravitino at the Fermilab Tevatron and CERN LEP colliders," *Phys. Rev. D*, vol. 54, pp. 5395-5411, Nov. 1996. C. Chen and J. Gunion, "Probing gauge-mediated supersymmetry breaking models at the Fermilab Tevatron via delayed decays of the lightest neutralino," *Phys. Rev. D*, vol. 58, pp. 075005-075016, Oct. 1998.

[6] F. Abe *et al.* (CDF Collaboration), "Searches for New Physics in Diphoton Events in $p\bar{p}$ Collisions at $\sqrt{s} = 1.8$ TeV," *Phys. Rev. Lett.*, vol. 81, pp. 1791-1796, Aug. 1998 and *Phys. Rev. D*, vol. 59, pp. 092002-092031, May 1999.

[7] In this thesis we assume a cylindrical coordinate system that defines z as the longitudinal axis along the proton beam, θ as the polar angle, ϕ as the azimuthal angle relative to the horizontal plane and $\eta = -\ln\tan(\theta/2)$. We take $E_T = E\sin\theta$ and $p_T = p\sin\theta$ where E is the energy measured by the calorimeter and p the momentum measured in the tracking system. If no vertex is reconstructed we use $z_{\text{collision}} = 0$. We define $\vec{\not\!\!E}_T = -\sum_i E_T^i \vec{n}_i$ where $\vec{n}_i$ is a unit vector in the transverse plane that points from the interaction vertex to the i^{th} calorimeter tower. $\not\!\!E_T$ is the magnitude of $\vec{\not\!\!E}_T$.

[8] P. Bode, J. Ostriker and N. Turok, "Halo Formation in Warm Dark Matter Models," *Astrophys. J.*, vol. 556, pp. 93-107, 2001.

[9] A. Abdulencia *et al.* (CDF Collaboration), "Search for Heavy Long-Lived Particles that Decay to Photons at CDF II," *Phys. Rev. Lett.*, vol. 99, pp. 121801-121808 7 pages, Sep. 2007. A. Abulencia *et al.*, (CDF Collaboration) "Search for Heavy, Long-Lived Neutralinos that Decay to Photons at CDF II Using Photon Timing," *arXiv*, hep-ex/0804.1043v1, 29 pages, Apr. 2008. Submitted to *Phys. Rev. D.*

[10] A. Heister *et al.* (ALEPH Collaboration), "Search for gauge mediated SUSY breaking topologies in $e^+ + e^-$ collisions at center-of-mass energies up to 209 GeV," *Eur. Phys. J. C*, vol. 25, pp.339-351, 2002. A. Garcia-Bellido, Ph.D. thesis, Royal Holloway University of London, England, 2002. also see M. Gataullin, S. Rosier, L. Xia and H. Yang, "Searches for Gauge-Mediated SUSY Breaking Topologies with the L3 Detector at LEP," *AIP Conf. Proc.*, vol. 903, pp. 217-220, Apr. 2007. OPAL Collaboration, "Search for Gauginos and Gauge Mediated SUSY Breaking Scenarios at LEP," *Proc. Sci. HEP2005*, Talk 346, 2006. DELPHI Collaboration, "Photon events with missing energy in $e^+ + e^-$ collisions at

$\sqrt{s}$= 130 to 209 GeV," *Eur. Phys. J. C*, vol. 38 No. 4, pp. 395-411, Jan. 2005.

[11] P. Wagner and D. Toback, "Prospects of searches for neutral, long-lived particles that decay to photons using timing at CDF," *Phys. Rev. D*, vol. 70, pp. 114032-114047, Dec. 2004.

[12] T. Aaltonen *et al.* (CDF Collaboration), "First Run II Measurement of the W Boson Mass," *arXiv*, hep-ex/0708.3642, 54 pages, Aug. 2007, Submitted to *Phys. Rev. D.*

[13] M. Goncharov *et al.*, "The Timing System for the CDF Electromagnetic Calorimeters," *Nucl. Instrum. Methods A*, vol. 565, pp.543-550, Sep. 2006.

[14] M. Goncharov, V. Krutelyov, D. Toback and P. Wagner, "Search for Heavy, Neutral Long-Lived Particles that Decay to Photons," *CDF Note*, Number 8016, 33 pages, Dec. 2006.

[15] B. Allanach *et al.*, "The Snowmass Points and Slopes: benchmarks for SUSY searches," *Eur. Phys. J. C*, vol. 25 No. 1, pp. 113-123, Sept. 2002. We take the messenger mass scale $M_{\rm M} = 2\Lambda$, $\tan(\beta) = 15$, $\mathrm{sgn}(\mu) = 1$ and the number of messenger fields $N_{\rm M} = 1$. The parameters $c_{\rm Grav}$ (gravitino mass factor) and Λ (supersymmetry breaking scale) are allowed to vary.

[16] D. Acosta *et al.* (CDF Collaboration), "Search for anomalous production of diphoton events with missing transverse energy at CDF and limits on gauge-mediated supersymmetry-breaking models," *Phys. Rev. D*, vol. 71, pp. 031104-031111, Feb. 2005. V. Abazov *et al.* (D0 Collaboration). "Search for Supersymmetry with Gauge-Mediated Breaking in Diphoton Events at D0," *Phys. Rev. Lett.*, vol. 94, pp. 041801 7 pages, Jan. 2005.

[17] The remaining processes produce slepton pairs that also decay to pairs of $\widetilde{\chi}_1^0$: τ_1 ($\sim 9\%$), e_R ($\sim 7\%$), μ_R ($\sim 7\%$).

[18] PYTHIA: T. Sjöstrand *et al.*, "High-energy-physics event generation with GEANT 6.1," *Comput. Phys. Commun.*, vol. 135, pp. 238-259, Apr. 2001. We use version 6.216.

[19] W. Beenakker *et al.*, "Production of Charginos, Neutralinos, and Sleptons at Hadron Colliders," *Phys. Rev. Lett.*, vol. 83, pp. 37803783, Nov. 1999.

[20] P. Simeon and D. Toback, "On Increasing the Sensitivity for Certain Types of Experiments to Search for New Elementary Particles," *Journ. of Undergrad. Phys.*, vol. 20, Aug. 2007.

[21] D. Acosta *et al.* (CDF Collaboration), "Limits on Extra Dimensions and New Particle Production in the Exclusive Photon and Missing Energy Signature in $p\bar{p}$ collisions at $\sqrt(s) = 1.96$ TeV," *Phys. Rev. Lett.*, vol. 89, pp. 281801-281808, Dec. 2002

[22] E. Boos, A. Vologdin, D. Toback and J. Gaspard, "Prospects of searching for excited leptons during run II of the Fermilab Tevatron," *Phys. Rev. D*, vol. 66, pp. 013011-013016, July 2002. J. Conway, "Setting Limits and Making Discoveries in CDF," *CERN Yellow Reports*, Report No. 2000-005, pp. 247-259, 2000.

CURRICULUM VITA

Education

- Texas A&M University- College Station, Texas
  Expected Graduation Date: May 2009
  Bachelor of Science in Physics and Bachelor of Science in Mathematics

Research

- Undergraduate Research Fellow (2007-2008)
  Office of Honors Programs, Texas A&M University
  Thesis Title: *Searching for Dark Matter in Particle Physics Experiments*
  Advisor: Dr. David Toback, Department of Physics

Leadership

- Dean's Student Advisory Panel member (2006-Present)
  College of Science, Texas A&M University

Honors

- Dean's List (2005-Present)
  College of Science, Texas A&M University
- 1^{st} place Freshman/Sophomore Math Competition (2006)
  Texas A&M University
- 1^{st} place Physics 218 Challenge Exam (2005)
  Texas A&M University
- President's Endowed Scholar (2005-Present)
  Texas A&M University
- Galen T. Brown Foundation Scholar (2005-Present)
  Texas A&M University

Talks

- "Paper Seminar for: Search for Heavy, Long-Lived Neutralinos that Decay to Photons at CDF II using Photon Timing," CDF Weekly Meeting
  Fermilab National Laboratory, April 2008
- "Figures Reblessing for: Search for Heavy, Long-Lived Neutralinos that Decay to Photons at CDF II using Photon Timing," CDF Exotics Meeting
  Fermilab National Laboratory, April 2008

- "Updated Figures for: Search for Heavy, Long-Lived Neutralinos in Gauge Mediated Supersymmetry Breaking Models Using Photon Timing at CDF II," CDF SUSY Meeting
  Fermilab National Laboratory, December 2007

- "Searches for a Dark Matter Candidate in Particle Physics Experiments at the Fermilab Tevatron," APS Texas Section Meeting
  Texas A&M University, October 2007

Publications

- SEARCH FOR HEAVY, LONG-LIVED NEUTRALINOS THAT DECAY TO PHOTONS AT CDF II USING PHOTON TIMING
  T. Aaltonen *et al.* (CDF Collagoration), Submitted to Physical Review D
  hep-ex/0804.1043